Journal of Alloys and Compounds 827 (2020) 154245

Contents lists available at ScienceDirect

Journal of Alloys and Compounds

journal homepage: http://www.elsevier.com/locate/jalcom

Review

Influence of phase composition and microstructure on corrosion behavior of laser based Ti–Co–Ni ternary coatings on Ti–6Al–4V alloy

Olanrewaju Seun Adesina [a, d, *], Babatunde Abiodun Obadele [b], Gabriel Ayokunle Farotade [a], Dayo Adeyemi Isadare [c], Adeolu Adesoji Adediran [d], Peter Pelumi Ikubanni [d]

[a] Department of Chemical, Metallurgical and Materials Engineering, Tshwane University of Technology, P.M.B. X680, Pretoria, 0001, South Africa
[b] Department of Chemical, Materials and Metallurgical Engineering, Botswana International University of Science and Technology, Palapye, Botswana
[c] Department of Materials Science and Engineering, Obafemi Awolowo University, Ile, Ife, Osun, Nigeria
[d] Department of Mechanical Engineering, Landmark University, P.M.B. 1001, Omu-Aran, Kwara, Nigeria

ARTICLE INFO

Article history:
Received 5 November 2019
Received in revised form
12 January 2020
Accepted 8 February 2020
Available online 10 February 2020

Keywords:
Ti-6Al–4V
Ti–Co–Ni
Laser cladding
Micro
Structure
Corrosion

ABSTRACT

Although Ti–6Al–4V alloy has wide applications in marine and chemical industries, its application is highly limited in corrosive environment such as sulphuric acid. This is due to the dissolution of the passive titanium hydride (TiH_2) film formed on the surface which accelerates the corrosion of titanium alloy in concentrated sulphuric acid. In this work, laser surface modification technique was used to develop high performance anti–corrosive coatings for aggressive sulphuric environment. The effects of parameter variations and volume fraction of Ti–Co–Ni clad layer on Ti–6Al–4V were investigated. The corrosion behaviors of Ti-6A-l4V, TiCo–10Ni and CoNi–10Ti coatings were studied in 0.5 M sulphuric acid using potentiodynamic polarization technique. Thereafter, the morphologies of the coatings before and after corrosion were analyzed using scanning electron microscope (SEM) equipped with energy dispersion spectroscopy (EDS) and X-ray diffraction (XRD) analysis to examine phase compositions and changes. The corrosion result shows that the clad compositions have significant influence on the potential by shifting the potential to more noble values and reduced the corrosion rate when compared with as-received Ti–6Al–4V. In addition, the corrosion resistance performance of CoNi–10Ti deposited at 1.2 m/min is best among all the ternary coated samples. The increase in corrosion resistance of alloys with cobalt and nickel on titanium is due to formation of dense passive CoO, TiO, TiAl, Ni_2TiO_3, V_2O_5 and Al_2O_3 oxides on the samples surfaces. With this result, the use of laser cladding technique could be established in improving the corrosion resistance of Ti–6Al–4V with Ti–Co–Ni alloy coatings.

Contents

* Corresponding author. Department of Chemical, Metallurgical and Materials Engineering, Tshwane University of Technology, P.M.B. X680, Pretoria, 0001, South Africa.
E-mail address: osaadesina@yahoo.com (O.S. Adesina).

https://doi.org/10.1016/j.jallcom.2020.154245
0925-8388/

1. Introduction

The development of new materials has been the driving force for technological advancement over the years. The need for new engineering materials is growing especially light metals such as aluminium, magnesium and titanium [1]. Ti−6Al−4V alloy, the workhorse of titanium alloys is uniquely characterized by desired and useful combination of exact bulk properties. These bulk properties which consist of low-density provide good strength to weight ratio, high specific strength and good corrosion resistance in many environmental conditions [2,3]. Other properties associated with Ti−6Al−4V alloy are elevated temperature resistance and biocompatibility [4,5]. As a result, Ti−6Al−4V alloy drives the material choice for marine (offshore) structures, aerospace and petrochemical industry [6]. Nevertheless, Ti−6Al4V alloy applications are restricted in aggressive corrosive environment such as chimney lining, titanium tube sheet and titanium tubes in offshore and gas plants [7,8]. According to Straumanis et al. [9], the potential of titanium in sulphuric acid becomes less noble (more anodic) in time, approaching a limiting potential and thus becomes less noble with increasing concentration of the acid. This is due to dissolution of protective stable and compact oxide film formed on titanium surface, hence, leading to a defective porous film and losing its protectiveness, especially in acidic solutions. According to Ban et al. [10], the protective films formed on the surface of titanium alloy are too thin and sometimes unstable to resist the shear stress and removed quickly, thus accelerating the metal dissolution. According to Wang et al. [11], the oxide film provides titanium the resistance to corrosion as long as the integrity of the film is maintained, although the potential difference of the $\alpha+\beta$ phase of Ti−6Al−4V could result in galvanic interaction and consequently act as special sites for deterioration to take place [12]. As a results, there is an increasing demand for new materials with greater properties to enhance service life and performance under harsh operating conditions for Ti6Al4V alloy.

Surface modification technique offers a way to improve surface properties and corrosion resistance of titanium alloy [4,13]. The surface alteration of materials through laser surface cladding technique which is a surface strengthening and repair technique is fast becoming more increasingly popular due to its significant progression in industrial applications [14]. Compared with other types of surface alteration methods, such as cold spraying, thermal spraying, magnetic sputtering and physical vapor deposition (PVD), laser cladding coatings technique have the advantages of dense microstructure, high precision, low dilution rate, strong metallurgical adhesion of the cladding material with the base material, limited heat effect due to controlled laser energy and rapid cooling [15,16]. Laser cladding of metallic alloys on titanium alloy has been used as an effective method to reduce the corrosion rate of titanium alloy in some extremely aggressive media. According to Tomashov [17], the following proposed mechanism such as cathodic alloying of metallic surface, the use of alloying element which increases passivity and the use of alloying element which can reduce thermal instability could be used to reduce the anodic activities of the titanium alloy.

According to Wang et al. [18], the corrosion resistance of titanium was improved by the addition of nickel-cobalt additives. Co−Ni coatings are essential in petrochemical plant owing to their low temperature super plasticity, high strength and anti-corrosion resistance [18−21]. For instance, nickel dissolves slowly in dilute acids and thus becomes passive with formation of passive oxide film in aggressive media while cobalt is an additive in many super alloys used for gas turbine engines, corrosion resistant alloys as well as catalysts for the petroleum and chemical industries. According to Zamani et al. [22], nickel could also resist corrosion even at elevated temperatures and for this reason it is used in gas turbines and rocket engines. Moreover, the addition of Ni [23] in laser cladding of Co is expected to produce complex phases of CoNi intermetallic with a wide range of superior and functional properties. Chai et al. [24] synthesized Co/Ni based alloy via electrodeposition technique and observed that appropriate cobalt and nickel content exerted various effects on performances such as refine grain that enhanced the corrosion resistance of the coatings.

There are few literatures available with respect to microstructural and corrosion behaviors of Ti−6Al−4V alloy in sulphuric environment. This research work focuses on fabrication on Ti−Co−Ni ternary alloy on Ti−6Al−4V via laser cladding technique. The microstructure and phases of the resultant coatings were analyzed using X-ray diffractometry (XRD) and scanning electron microscopy (SEM) equipped with energy dispersive spectrometry (EDS) while the electrochemical technique using linear potentiodynamic polarization was used to evaluate the corrosion behavior of TiCoNi/Ti−6Al−4V alloy in 0.5 M H_2SO_4.

2. Experimental procedure

2.1. Materials

Grade 5 Ti−6Al−4V alloy specimens with dimension of 50 × 50 × 5 mm were sandblasted with silica grit sand and cleaned with acetone prior to laser cladding process in order to minimize laser reflection and increase the laser absorption on titanium alloy [25,26]. Titanium (Ti), cobalt (Co), and nickel (Ni) powders (99.9% purity and average particle size of 45 μm supplied by TLS Technik GmBH and Co (Bitterfeld-Wolfen, Germany) were premixed and homogenized in a Turbula shaker mixer T2F using a 250 ml air-tight

Table 1
Laser processing parameters of TiCo−Ni and CoNi−10Ti Ternary coatings.

Sample	Clad material	Power (W)	Scan speed (m/min)	Beam diameter (mm)	Powder feed rate (g/min)	Gas flow rate (L/min)
A	TiCo−10Ni	900	0.6	3	1.0	1.2
B	TiCo−10Ni	900	1.2	3	1.0	1.2
C	CoNi−10Ti	900	0.6	3	1.0	1.2
D	CoNi−10Ti	900	1.2	3	1.0	1.2

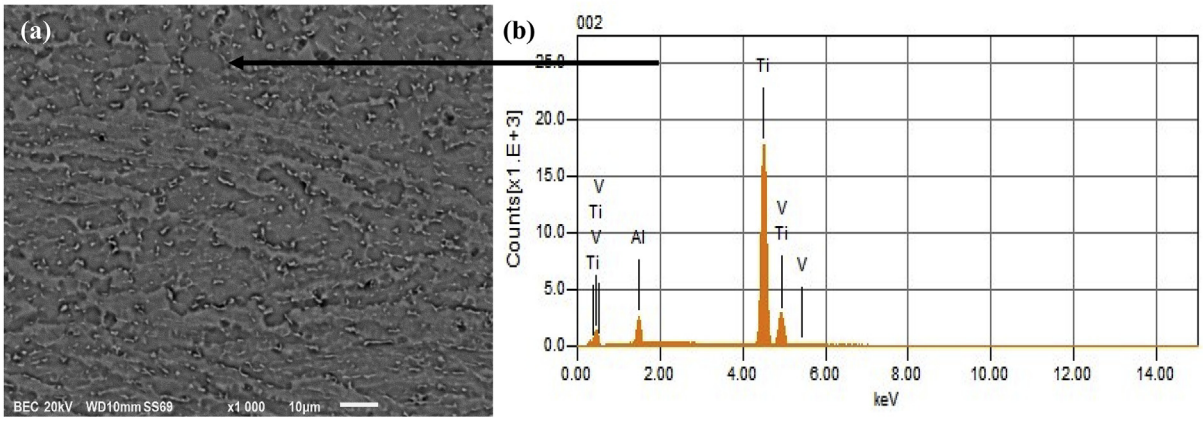

Fig. 1. (a) SEM Morphology and (b) EDS of Ti−6Al−4V alloy.

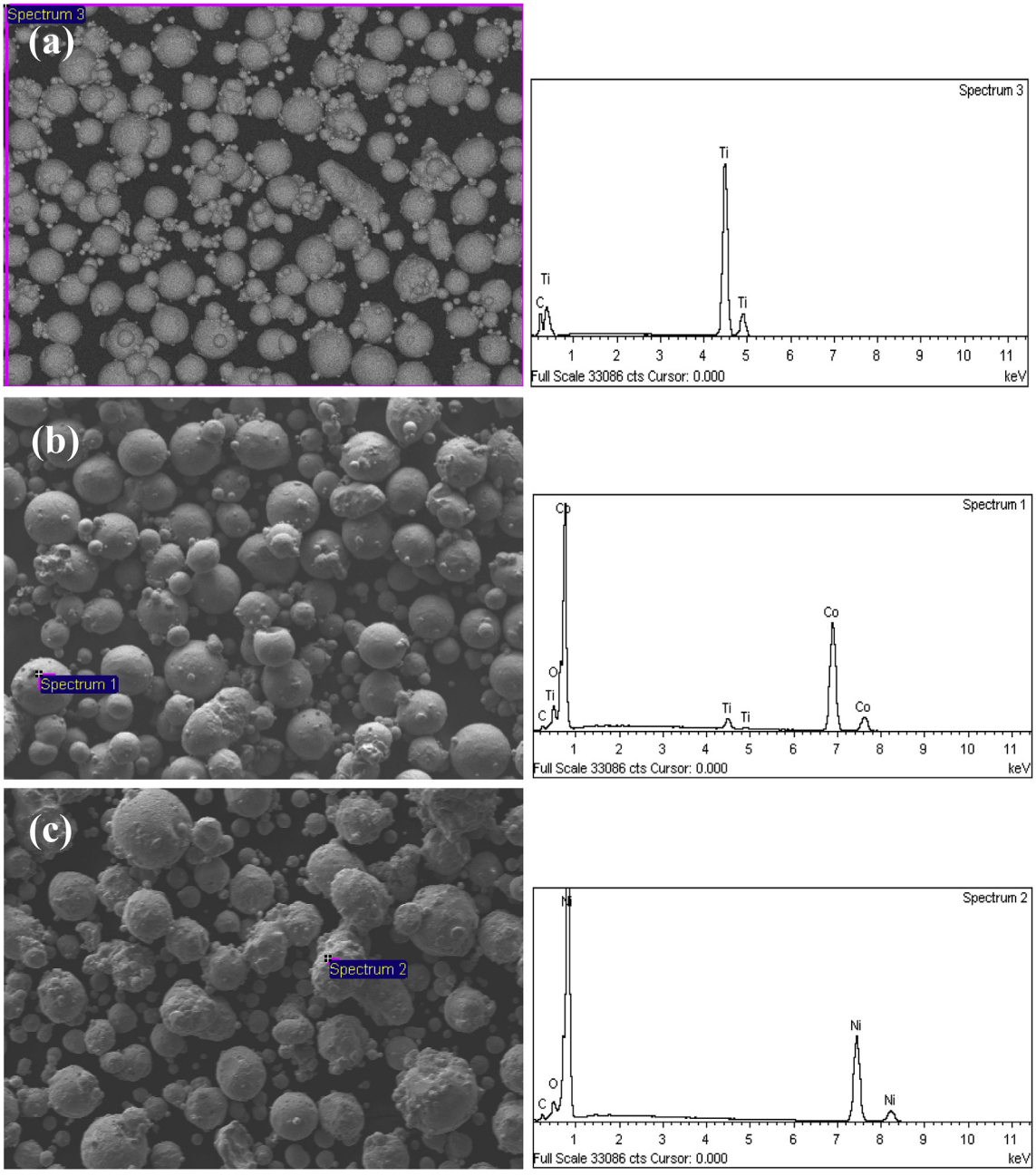

Fig. 2. SEM/EDS reveals morphologies of (a) Ti (b) Co and (c) Ni powders.

cylindrical plastic container with a fill level of 25% of the loaded powders. The mixing container was place in the chamber and subsequent procedures were followed as reported by Obadele et al. [27]. The Turbula mixing speed and duration utilized were 49 rpm and 8 h respectively. The mixing of the powders was done in a dry environment and at room temperature in order to prevent inhomogeneous mixture, which may result in irregular flowability of the powders during laser cladding process [27].

2.2. Laser processing

A 4.4 kW Rofin Sinar DY044, Continuous Wave Nd:YAG laser equipped with KUKA articulated arm robotic system was used to clad admixed Ti–Co–Ni powders on Ti–6Al–4V alloy. The deposited powders were infused in an admixed proportion into the melt pool formed by the laser beam during scanning of the substrate. The laser parameters were optimized at laser power of 900 W, powder feed rate 1.0 g/min, gas flow rate 1.2 L/min and beam spot size 3 mm. The scan speeds were varied from 0.6 to 1.2 m/min. In order to achieve coatings with large surface area, multiple clad tracks were deposited with 50% overlap at an angle of 45° to the substrate. Argon gas of 3 L/min was used during deposition to create a non-oxidizing atmosphere around the molten pool. This was done to avert oxidation, taken into consideration that titanium has high affinity for oxygen. Table 1 summarizes the laser cladding parameters utilized for deposition of Ti–Co–Ni coatings on Ti–6Al–4V alloy.

2.3. Characterization of laser coatings

After laser cladding, coatings for microstructural characterization were ground using P80, P320, P1200 and P4000 grit SiC grinding papers on a Struer TegraForce-25 automated diamond suspension dispenser. Thereafter, the clad samples were polished on a MD-Largo and refined with a MD-Chem OP-S polishing cloth with a Diapro diamond suspension respectively. During metallography preparation care was taken not to grind off the coatings on the surface. Subsequently, the polished samples were etched in Kroll's reagent (92 ml H_2O, 6 ml HNO_3 and 2 ml HF) for approximately 10 s prior to characterization to avoid over-etching. The etching was done for distinctive precision of microstructural phases present.

A Jeol JSM-7600F field emission scanning electron microscope (FESEM) was employed to study the morphologies of the laser clad coatings while elemental compositions were identified by energy dispersive spectroscopy (EDS). A Philips PW1713 X-ray diffractometer (XRD) equipped with monochromatic Cu Kα radiation set at 40 kV and 20 mA was used to collect diffraction peaks. Philips Analytical X'Pert High Scores software coupled with an in-built (ICSD) database was subsequently used for phase identification. The scan range was between 10° and 80° at 2 theta (2θ) and a step size of 0.02°.

2.4. Electrochemical test

Specimens for electrochemical test were sectioned to 1 cm^2, thereafter, an insulated copper cable was attached using aluminium tape to one face of the specimen. The specimens were ground to surface finish with 1200-grit SiC papers and polished to 3 mm using diamond suspension. Furthermore, the specimens were ultrasonically cleaned in ethanol before immersion in 0.5 M H_2SO_4 acid solution for corrosion test. Electrochemical measurements were conducted using an Autolab Potentiostat (PGSTAT302) which is computer controlled. The experiments were conducted using the three-electrode corrosion cell setup with saturated silver/silver chloride electrode (Ag/AgCl) (3 M KCl) as reference electrode while graphite rod served as counter electrode and the sample as working electrode. The corrosion potential (Ecorr), corrosion current density (Icorr), polarization resistance (Rp) and corrosion rate were calculated using the Tafel extrapolation method. A scan rate of 2 mV s^{-1} was initiated at a potential range between −1.5 and 2.0 V. Prior to starting the potentiodynamic polarization scan, the specimens were cathodically polarized at −1000 mV for 5 min followed by open circuit potential measurement for about 60 min. In all cases, triplicate experiments were carried out to ensure reproducibility. Similar procedure is reported by Obadele et al. [4,26].

3. Result and discussions

Fig. 1 represents SEM and EDS of Ti–6Al–4V alloy. According to Mokgalaka et al. [12], the material structure consist of alpha and beta (α+β) phases, where the α phase is characterized by HCP crystal structure and β phase with a BCC crystal structure. Fig. 2 reveals the morphologies of the as-received powders. The powders are spherical and non-porous with significant amount of satellites, indicating that the method of powder production is by gas atomization [1].

Fig. 3 presents the microstructural evolution of synthesized TiCo–10Ni coatings at laser speeds of 0.6 m/min and 1.2 m/min both at 900 W. According to Weng et al. [28], the difference in microstructural evolution of the synthesized coatings was as a result of variation of scan speed which mostly results in unique solidification rates. Both fabricated coatings as shown in Fig. 3(a) and (b) resulted in homogenous grains, free from pores and cracks or no initiation of stress. As shown in Fig. 3(a), the formation of larger grain size was observed as a result of longer interaction between heated powders and the absorbing energy while at high scan speed of 1.2 m/min (see Fig. 3(b)) the micrograph indicate small grain size and formation of dendritic grain shape as a result of fast cooling of the melt pool during solidification process [29]. The interaction of powders while travelling from the nozzle with the laser beam resulted in absorption of heat from the laser source. This time-factor interaction could affect the final grain size produced. According to Tamanna et al. [30], heat transfer from laser beam to powders is governed by the following equation.

$$1 \Big/ 3r_p\rho_p C_p dT \Big/ dt = 1 \Big/ 4\left(I_{dir} + I_{ref}\right)\eta_p - h(T_{-\infty}) - \varepsilon\sigma\left(T^4 - T_{\infty}^4\right) - 1 \Big/ 3\rho L_f rp1 \Big/ dt \quad (1)$$

where r_p is the radius of particle, ρ_p is the density of the particle, C_p is the specific heat of powder, I_{dir} and I_{ref} are the energy coming from laser beam on the particle and reflected from substrate respectively, ρ_p is the absorption coefficient of particle, h is the heat convection coefficient, T is the temperature of particle, T_∞ is the temperature of the surrounding gas, ε is the particle emissivity and L_f is the latent heat of fusion. The EDS of the laser clad samples (see Fig. 3) shows the presence of elemental Ti, Co, Ni and Al which is

different from that of the control titanium alloy. The presence of these elemental compounds indicates the prolong interaction time between the laser beam and melt pool as a result of lower laser scan speed as well as complete deposition on Ti–6Al–4V surface [31].

On the other hand, Fig. 4 shows the morphology of CoNi–10Ti coatings at different laser scan speed. The microstructure displayed flower-like dendritic structures at various laser scan speeds. The inter–diffusion of atoms from the coatings and the substrate as a result of high temperature gradient and solidification rate resulted in the formation of flower-like structures. Larger size of flower–like dendrite with dark grey coloration was observed at lower scan speed as a result of precipitate diffusion. However, at high scan speed insufficient diffusion occurred leading to white grey colored flower–like dendrite. Furthermore, as a result of combining binary and ternary phases, there could be the formation of laves phases which may account for the presence of intermetallic phases after laser cladding, as high temperature from the laser source is involved in newer phases being formed. According to Liu et al. [32], laves phase could form as a result of high amount of CoNi at high temperatures. In addition, the SEM micrographs revealed dark unmelted particles of the powders deposited on the coating. According to Shuja and Yilbas [33], the high convective effect associated with laser beam could impede complete melting of the powders at free surfaces of the substrate. Generally, the powder compositions significantly influence the microstructural evolution and phases formed during laser surface cladding.

Fig. 5 shows the XRD patterns of various intermetallic phases formed as a results of laser beam interaction on the cladding material and the substrate. Fig. 5(a) displays XRD results for TiCo–10Ni coatings at 0.6 m/min scan speed. The intermetallic phases of Al_2Ti, CoTi, Al_5Co_2, Ni_3Ti and $AlTi_3$, were identified as main peak. Major diffractions peaks of 34.25°, 42.08°, 43.29°, 54.27° and 78.65° and their inter-planar distance of 2.146 Å, 2.089 Å, 2.073 Å, 1.682 Å and 1.215 Å respectively. Meanwhile intermetallic phases of $AlTi_2$, Al_5Co_2, Ti_2Ni, Ni_4Ti, Co_2Ti and Ni_3Ti were formed at major diffraction peaks of 42.06°, 43.25°, 51.09°, 57.12°, 62.40° and 78.25°, the inter-planar distance of 2.189 Å, 2.147 Å, 2.136 Å, 2.090 Å, 1.806 Å and 1.487 Å for TiCo–10Ni coating at laser scan of 1.2 m/min scan speed as shown in Fig. 5(b). The synthesized hard phases observed in Figs. 4 and 5 could be associated with high temperature gradients [25,31,34–37].

In comparison, Fig. 5(c) reveals the XRD spectrum of CoNi–10Ti intermetallic coatings at 0.6 m/min scan speed. The main phase constituents of the coatings deposited at 0.6 m/min are NiTi, Ni_3Ti, $AlTi_2$, Co_2Ti, Al_5Co_2, $AlCo_2Ti$ and Ni_5Al_3. Major diffractions peaks are located at peak positions 34.25°, 42.08°, 43.29°, 54.27° and 78.65° with inter-planar distance of 2.146 Å, 2.089 Å, 2.073 Å, 1.682 Å and 1.215 Å respectively. On the other hand, Ni_3Ti, $AlTi_2$, Al_5Co_2, Co_2Ti, and CoTi predominate the coating at 1.2 m/min as shown in Fig. 5(d) with major diffraction peaks of 25.11°, 25.72°, 45.90° and 48.1° with inter-planar distance; 2.51 Å, 2.92 Å, 3.37 Å and 3.77 Å respectively. At CoNi–10Ti ternary coatings, the major intermetallic peaks deposited at 0.6 m/min were Co_2Ti, $AlTi_2$, TiCo, Ni_3Ti and Al_5Co_2, while intermetallic phases of Co_2Ti, TiCo and Ni_3Ti

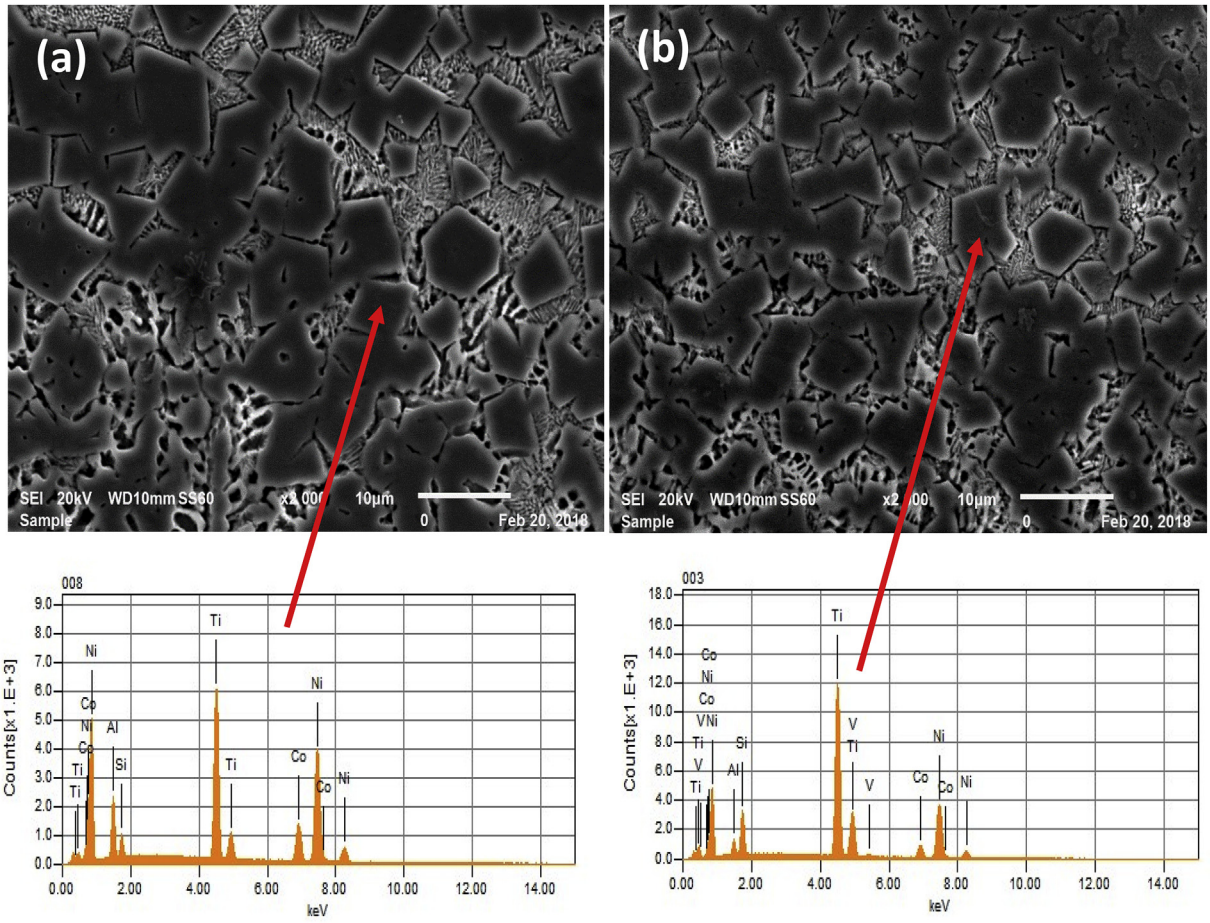

Fig. 3. SEM micrographs and EDS of laser cladded TiCo–10Ni Coatings at (a) 0.6 m/min and (b) 1.2 m/min.

predominate the coating at 1.2 m/min. It was evident that no single oxide of nickel, cobalt or titanium or any other metallic oxide was formed due to effective shielding during laser cladding process. In addition, the high energy radiated by the laser beam lead to molten powders interactions with substrate, thereby yielding complex chemical reactions. The combination of ductile NiTi martensitic phase and Ni_3Ti phase could influence the corrosion response of the coatings. Figs. 4–7 also indicates the presence of $AlTi_2$. According to Kaibyshev, Mazurina and Gromov [38], the addition of titanium as grain refinement plays a critical role in formation of aluminium rich in aluminium-titanium ($AlTi_2$) phase [39,40].

Fig. 6 illustrates the potentiodynamic linear polarization curves of Ti–Co–10Ni and Co–Ni–10Ti laser cladded on Ti–6Al–4V substrate at scan speeds 0.6 and 1.2 m/min respectively in 0.5 M H_2SO_4. Tafel extrapolation technique was used to derive the corrosion results summarized in Table 2. It could be observed that the cathodic branches of the linear polarization curves for the Ti–6Al–4V alloy and all the ternary coatings exhibit current densities that decrease as the applied potential increases. Also, the Ti–6Al–4V alloy (substrate) as well as the coatings displayed similar anodic branch behaviour, although, Co–Ni–10Ti deposited at 0.6 m/min showed formation of metastable pits which could be associated with the slight passivation trend and re-passivation of micro-size pits on the surface of the coating.

As presented in Table 2, TiCo–10Ni coated at low 0.6 m/min speed exhibited polarization resistance Rp (1543 Ω cm^2), corrosion current density I_{corr} (9.24 μA/cm^2), and corrosion rate Cr (0.0812 mm/year). Lower I_{corr} value observed for Ti–Co–10Ni lased at 1.2 m/min speed suggests an improvement in corrosion resistance with increase in polarization resistance Rp (1633.45 Ω cm^2), decrease in corrosion current density I_{corr} (8.73 μA/cm^2), and decrease in corrosion rate Cr (0.0767 mm/year). The addition of Ni to titanium matrix exhibited superior corrosion as a result of passive film formed on the surface of the coating, thus, reducing the release of metal ions from the coatings to the solution. In addition, enhanced corrosion properties displayed by the addition of nickel to the fabricated coatings could be associated with the presence of Ni–Ti phase which is nobler than Ti–6Al–4V [12]. According to Hu et al. [41], protective film on the coating surface helps to slow down or stop accelerated electrochemical surface deterioration.

As observed for CoNi–10Ti ternary coatings, an increase in laser scan speed resulted in corrosion current density of the fabricated coatings declining from 0.79 μA/cm^2 to 0.000922 μA/cm^2, thus revealing the effect of laser speed on corrosion current by changes in the grain size. Co–Ni–10Ti coatings at high scan speed of 1.2 m/min exhibited lowest corrosion rate (8.09E-06 mm/yr), as well as highest polarization resistance Rp (1.55E07 Ω cm^2). Compared to the Ti–6Al–4V alloy (substrate), the corrosion resistance property

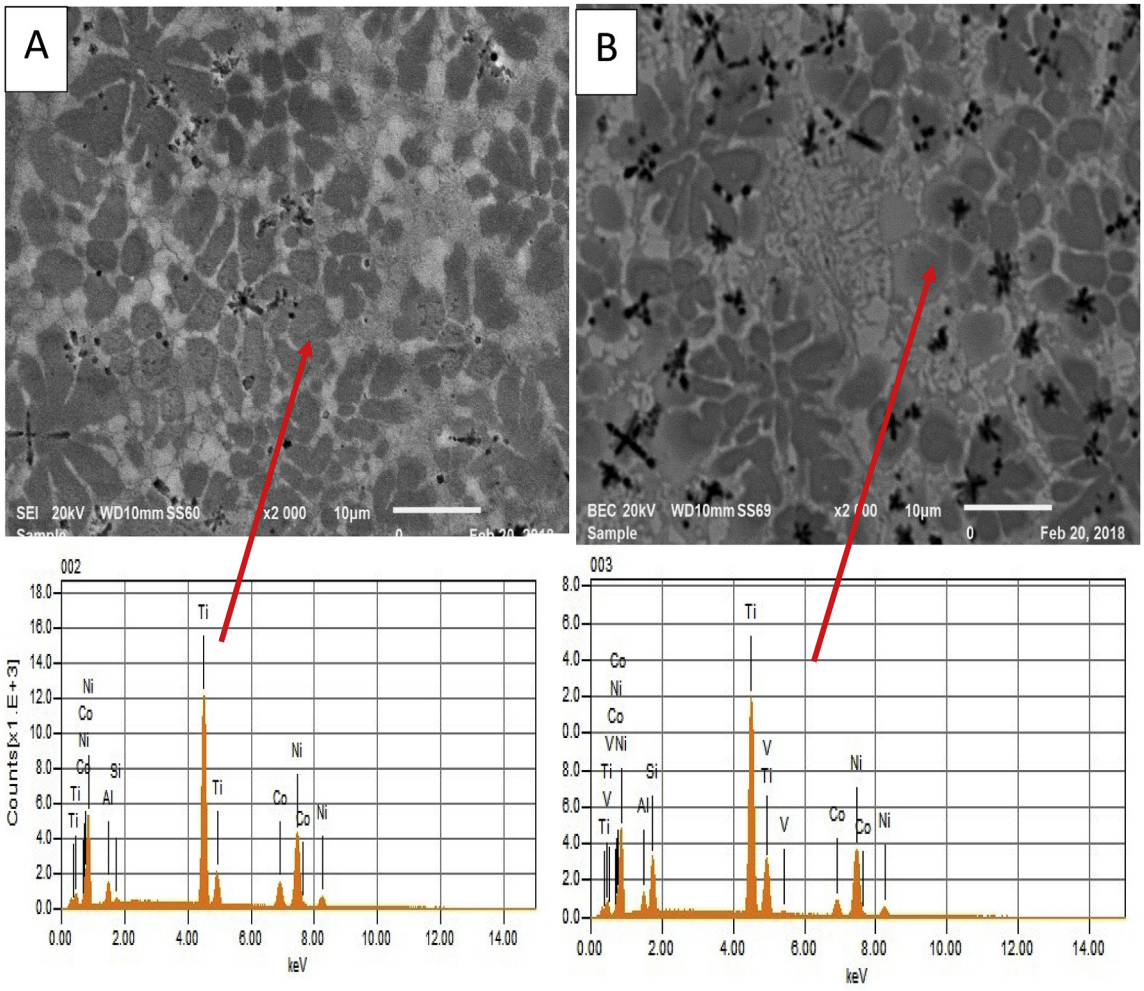

Fig. 4. SEM and EDS micrographs showing coatings of CoNi–10Ti coatings at (a) 0.6 m/min and (b) 1.2 m/min.

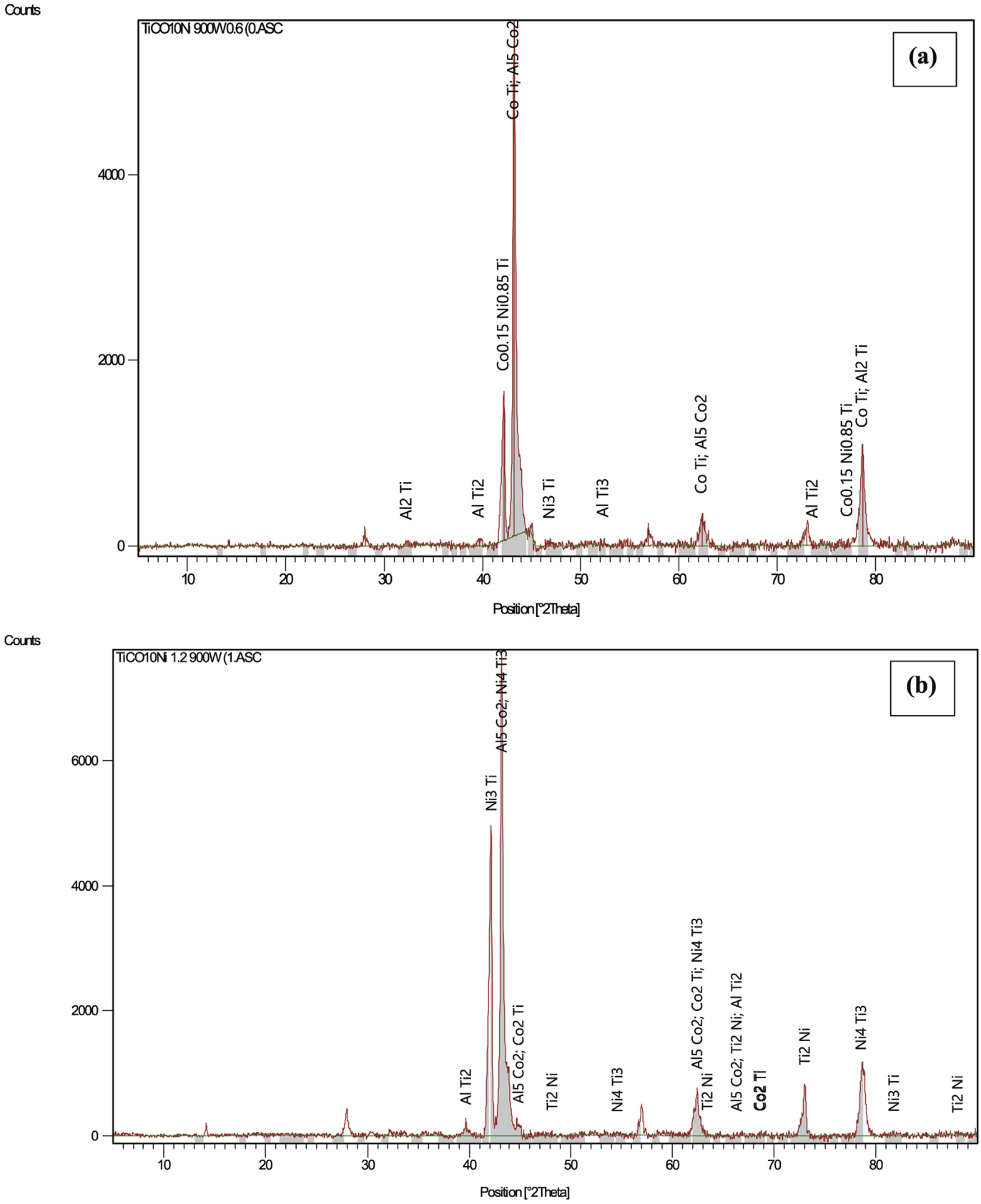

Fig. 5. XRD spectrum of laser clad TiCo−10Ni coating at (a) 0.6 m/min, (b) 1.2 m/min and laser clad CoNi−10Ti at (c) 0.6 m/min, (d) 1.2 m/min.

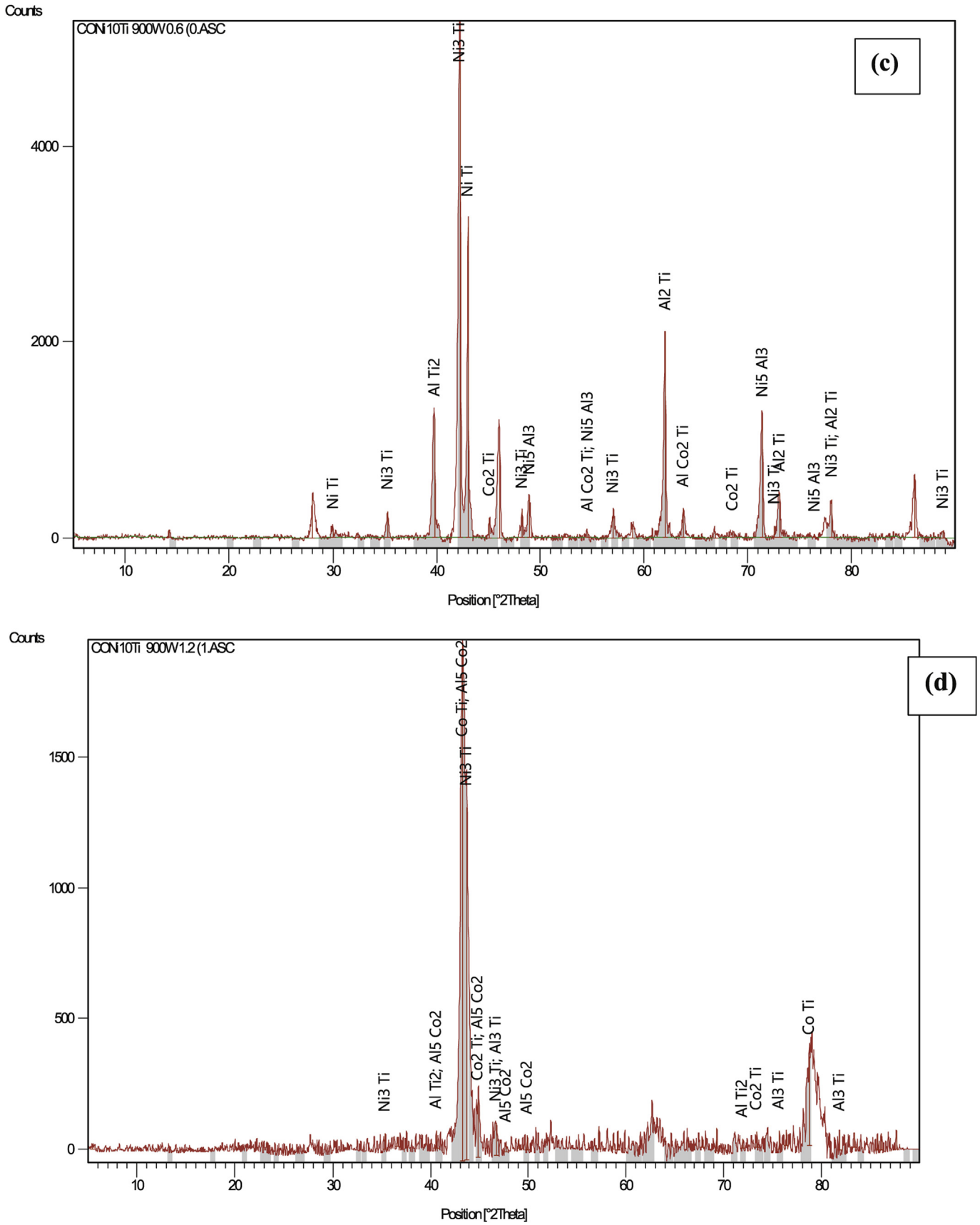

Fig. 5. (*continued*).

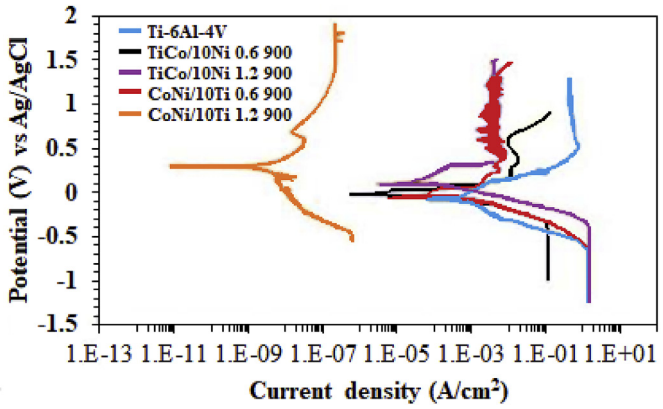

Fig. 6. Linear polarization curves of Ti–Co–10Ni and Co–Ni–10Ti ternary coated Ti–6Al–4V in 0.5 M H_2SO_4 solution.

of clad samples improved when CoNi–10Ti was added. According to Tomashov [42], the use of alloying elements such as cobalt and nickel can be used to reduce thermodynamic instability as well as increase the passivity of titanium. These alloying elements are usually employed to enhance the corrosion resistance of titanium for a spontaneous passive system. Generally, cladding of Ti–6Al–4V with TiCO and/or CoNi significantly improves the corrosion performance of Ti–6Al–4V.

The increase in corrosion resistance of alloys with cobalt and nickel on titanium is due to formation of thick passive TiO_2, Co_3O_4, NiO and CoO formed on the sample surface [43–45]. This could be justified by the in the formation of protective oxides as shown in Fig. 7.

Fig. 8 shows the XRD spectra of dense passive oxide layers formed on the surface of the coatings after immersion in 0.5 M H_2SO_4. There was significant reduction in the corrosion rates of all the coated samples due to the oxide films formed on the laser coated Ti–6Al–4V alloy samples. The oxides revealed at these

Table 2
Corrosion test results for TiCo–10Ni and CoNi–10Ti ternary coatings.

Sample	E_{corr} (V)	I_{corr} (μA.cm^{-2})	R_p (Ω.cm^2)	CR (mm.yr^{-1})
Ti–6Al–4V	−0.18	102	139.8	0.896
TiCo–10Ni (0.6)	−0.12	9.24	1543.29	0.0812
TiCo–10Ni (1.2)	+0.18	8.73	1633.45	0.0767
CoNi–10Ti (0.6)	−0.15	0.79	18165.6	0.0069
CoNi–10Ti (1.2)	+0.23	0.000922	1.55E07	8.09E-06

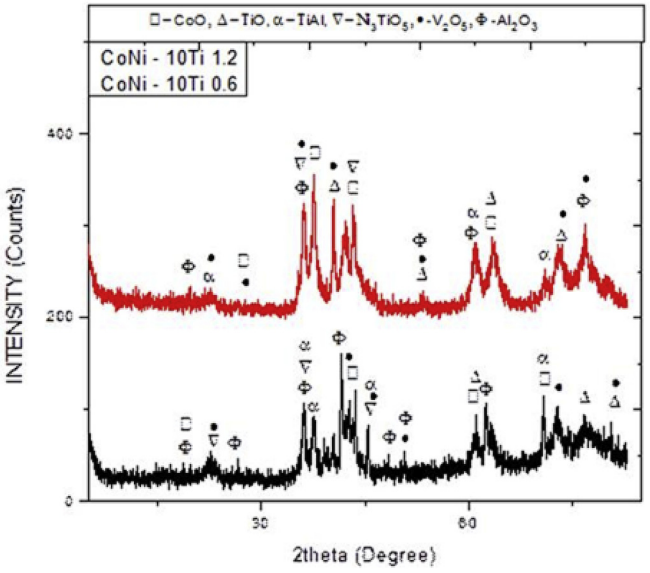

Fig. 8. XRD spectra of CoNi–10Ti ternary coatings after corrosion.

peaks are CoO, TiO, TiAl, Ni_2TiO_3, V_2O5 and Al_2O_3. During high temperature processing of Ti–6Al–4V, the precipitation of Ti–Al intermetallics (TiAl) had been reported as seen in Fig. 8. Titanium

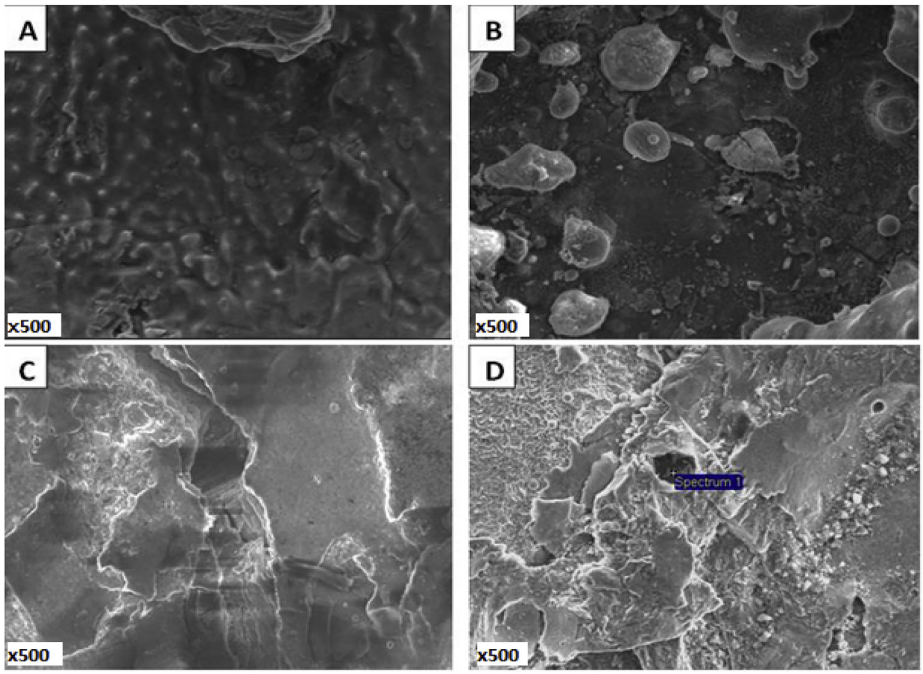

Fig. 7. SEM morphology of the coated samples after corrosion (a) Ti–Co–10Ni –0.6 (b) Ti–Co–10Ni –1.2 (c) Co–Ni–10Ti –0.6 (d) Co–Ni–10Ti –1.2.

aluminides are ordered intermetallics with strong bonding of the compounds and high critical ordering temperature (Tc) of the material which gives rise to good thermochemical properties and good structural stability [46]. Ti and Ti−Al alloys are more highly permeable to oxygen, and Al has a low diffusivity in lower aluminium containing alloys [47]. Fig. 8 reveals TiO which is more stable than Al_2O_3. The thermodynamic stabilities of the oxides of Ti and Al are quite similar, thus establish an Al_2O_3 scale due to the competition from TiO.

4. Conclusion

In this study, CoNi−10Ti and TiCo−10Ni were successfully fabricated on Ti6Al4V by laser cladding route with scan speed of 0.6 m/min and 1.2 m/min at 900 W respectively. The following conclusions are drawn from the work.

(1) Coatings revealed microstructures of high quality with no evidence of porosity, crack or initiation of stress. A strong metallurgical adhesion was also obtained between the coatings and substrate interface.
(2) At CoNi−10Ti ternary coatings, the major intermetallic peaks deposited at 0.6 m/min were Co_2Ti, $AlTi_2$, Ti−Co, Ni_3Ti and Al_5Co_2, while intermetallic phases of Co_2Ti, Ti−Co and Ni_3Ti predominate the coating at 1.2 m/min. It was evident that no single oxide of nickel, cobalt or titanium or any other metallic oxide was formed due to effective shielding during laser cladding process. In addition, the high energy radiated by the laser beam lead to molten powders interactions with substrate, thereby yielding complex chemical reactions.
(3) Co−Ni−10Ti coatings at high scan speed of 1.2 m/min exhibited lowest corrosion rate Cr (8.09E-03 mm/yr), lowest corrosion current density Icorr (0.000922 $\mu A/cm^2$) as well as highest polarization resistance Rp (1.55E+07 $\Omega\ cm^2$), which is 110872 times the polarization resistance of the Ti−6Al−4V.
(4) The corrosion resistance performance of Co−Ni−10Ti deposited at 1.2 m/min is best among all the ternary coated samples. The increase in corrosion resistance of alloys with cobalt and nickel on titanium could be associated to formation of dense passive CoO, TiO, TiAl, Ni_2TiO_3, V_2O5 and Al_2O_3 oxides on the sample surface.

Declaration of competing interest

The authors declare that they have no known competing financial interests or personal relationships that could have appeared to influence the work reported in this paper.

Acknowledgment

This research is supported by the National Laser Centre (NLC), Council for Scientific and Industrial Research (CSIR), Pretoria, South Africa.

References

[1] B.A. Obadele, O.O. Ige, P.A. Olubambi, Fabrication and characterization of titanium-nickel-zirconia matrix composites prepared by spark plasma sintering, J. Alloys Compd. 710 (2017) 825−830.
[2] M. Savalani, C. Ng, Q. Li, H. Man, In situ formation of titanium carbide using titanium and carbon-nanotube powders by laser cladding, Appl. Surf. Sci. 258 (2012) 3173−3177.
[3] B.A. Obadele, P.A. Olubambi, A. Andrews, S. Pityana, M.T. Mathew, Electrochemical behaviour of laser-clad Ti6Al4V with CP Ti in 0.1 M oxalic acid solution, J. Alloys Compd. 646 (2015) 753−759.
[4] B.A. Obadele, P.A. Olubambi, A. Andrews, S. Pityana, M.T. Mathew, Electrochemical behaviour of laser-clad Ti6Al4V with CP Ti in 0.1 M oxalic acid solution, J. Alloys Compd. 646 (2015) 753−759.
[5] L. Semetse, B.A. Obadele, L. Raganya, J. Geringer, P.A. Olubambi, Fretting corrosion behaviour of Ti-6Al-4V reinforced with zirconia in foetal bovine serum, J. Mech. Behav. Biomed. Mater. (2019) 103392.
[6] A.O. Adegbenjo, B.A. Obadele, P.A. Olubambi, Densification, hardness and tribological characteristics of MWCNTs reinforced Ti6Al4V compacts consolidated by spark plasma sintering, J. Alloys Compd. 749 (2018) 818−833.
[7] I. Gurrappa, Characterization of titanium alloy Ti-6Al-4V for chemical, marine and industrial applications, Mater. Char. 51 (2003) 131−139.
[8] R. Schutz, H. Watkins, Recent developments in titanium alloy application in the energy industry, Mater. Sci. Eng., A 243 (1998) 305−315.
[9] M.E. Straumanis, P.C. Chen, The corrosion of titanium in acids—the rate of dissolution in sulfuric, hydrochloric, hydrobromic and hydroiodic acids, Corrosion 7 (1951) 229−237.
[10] S. Ban, Y. Iwaya, H. Kono, H. Sato, Surface modification of titanium by etching in concentrated sulfuric acid, Dent. Mater. 22 (2006) 1115−1120.
[11] Z.B. Wang, H.X. Hu, Y.G. Zheng, W. Ke, Y.X. Qiao, Comparison of the corrosion behavior of pure titanium and its alloys in fluoride-containing sulfuric acid, Corrosion Sci. 103 (2016) 50−65.
[12] M.N. Mokgalaka, S.L. Pityana, P.A.I. Popoola, T. Mathebula, NiTi intermetallic surface coatings by laser metal deposition for improving wear properties of Ti-6Al-4V substrates, Adv. Mater. Sci. Eng. 2014 (2014) 8.
[13] A. Bloyce, P.Y. Qi, H. Dong, T. Bell, Surface modification of titanium alloys for combined improvements in corrosion and wear resistance, Surf. Coating. Technol. 107 (1998) 125−132.
[14] B.A. Obadele, A. Andrews, M.T. Mathew, P.A. Olubambi, S. Pityana, Improving the tribocorrosion resistance of Ti6Al4V surface by laser surface cladding with TiNiZrO 2 composite coating, Appl. Surf. Sci. 345 (2015) 99−108.
[15] F. Weng, C. Chen, H. Yu, Research status of laser cladding on titanium and its alloys: a review, Mater. Des. 58 (2014) 412−425.
[16] B. Cárcel, A. Serrano, J. Zambrano, V. Amigó, A.C. Cárcel, Laser cladding of TiAl intermetallic alloy on Ti6Al4V -process optimization and properties, Physics Procedia 56 (2014) 284−293.
[17] N. Tomashov, R. Altovsky, G. Chernova, Passivity and corrosion resistance of titanium and its alloys, J. Electrochem. Soc. 108 (1961) 113−119.
[18] L. Wang, Y. Gao, Q. Xue, H. Liu, T. Xu, Microstructure and tribological properties of electrodeposited Ni−Co alloy deposits, Appl. Surf. Sci. 242 (2005) 326−332.
[19] M.A. Farzaneh, K. Raeissi, M.A. Golozar, Effect of current density on deposition process and properties of nanocrystalline Ni−Co−W alloy coatings, J. Alloys Compd. 489 (2010) 488−492.
[20] G.D. Hibbard, K.T. Aust, U. Erb, Thermal stability of electrodeposited nanocrystalline Ni−Co alloys, Mater. Sci. Eng., A 433 (2006) 195−202.
[21] M. Srivastava, V. Ezhil Selvi, V.K. William Grips, K.S. Rajam, Corrosion resistance and microstructure of electrodeposited nickel−cobalt alloy coatings, Surf. Coating. Technol. 201 (2006) 3051−3060.
[22] M. Zamani, A. Amadeh, S.M. Lari Baghal, Effect of Co content on electrodeposition mechanism and mechanical properties of electrodeposited Ni−Co alloy, Trans. Nonferrous Metals Soc. China 26 (2016) 484−491.
[23] Y.-z. Zhang, Y. Tu, M.-z. Xi, L.-k. Shi, Characterization on laser clad nickel based alloy coating on pure copper, Surf. Coating. Technol. 202 (2008) 5924−5928.
[24] Z. Chai, C. Jiang, Y. Zhao, C. Wang, K. Zhu, F. Cai, Microstructural characterization and corrosion behaviors of Ni-Cu-Co coatings electrodeposited in sulphate-citrate bath with additives, Surf. Coating. Technol. 307 (2016) 817−824.
[25] O.S. Adesina, A. Mthisi, A.P.I. Popoola, The effect of laser based synthesized Ti-Co coating on microstructure and mechanical properties of Ti6al4v alloy, Procedia Manuf. 7 (2016) 46−52.
[26] B.A. Obadele, A. Andrews, M.T. Mathew, P.A. Olubambi, S. Pityana, Improving the tribocorrosion resistance of Ti6Al4V surface by laser surface cladding with TiNiZrO2 composite coating, Appl. Surf. Sci. 345 (2015) 99−108.
[27] B.A. Obadele, Z.H. Masuku, P.A. Olubambi, Turbula mixing characteristics of carbide powders and its influence on laser processing of stainless steel composite coatings, Powder Technol. 230 (2012) 169−182.
[28] F. Weng, H. Yu, C. Chen, J. Liu, L. Zhao, J. Dai, Microstructure and property of composite coatings on titanium alloy deposited by laser cladding with Co42+TiN mixed powders, J. Alloys Compd. 686 (2016) 74−81.
[29] Y. Sun, M. Hao, Statistical analysis and optimization of process parameters in Ti6Al4V laser cladding using Nd:YAG laser, Optic Laser. Eng. 50 (2012) 985−995.
[30] N. Tamanna, R. Crouch, S. Naher, Progress in numerical simulation of the laser cladding process, Optic Laser. Eng. 122 (2019) 151−163.
[31] H. Alemohammad, S. Esmaeili, E. Toyserkani, Deposition of Co−Ti alloy on mild steel substrate using laser cladding, Mater. Sci. Eng., A 456 (2007) 156−161.
[32] R. Liu, S. Xi, S. Kapoor, X. Wu, Effects of chemical composition on solidification, microstructure and hardness of Co-Cr-W-Ni and Co-Cr-Mo-Ni alloy systems, Int. J. Res. Rev. Appl. Sci. 5 (2010) 110−122.
[33] S.Z. Shuja, B.S. Yilbas, Laser produced melt pool: influence of laser intensity parameter on flow field in melt pool, Optic Laser. Technol. 43 (2011) 767−775.
[34] Y. Xue, H.M. Wang, Microstructure and dry sliding wear resistance of CoTi intermetallic alloy, Intermetallics 17 (2009) 89−97.
[35] A.V. Davydov, U.R. Kattner, D. Josell, R.M. Waterstrat, W.J. Boettinger, J.E. Blendell, A.J. Shapiro, Determination of the CoTi congruent melting point

and thermodynamic reassessment of the Co-Ti system, Metall. Mater. Trans. 32 (2001) 2175–2186.
[36] S. Anada, A. Zensho, H. Yasuda, H. Mori, Phase change of CoTi and Co3Ti induced by MeV-scale electron irradiation, Phil. Mag. 96 (2016) 2027–2039.
[37] F. Cai, C. Jiang, P. Fu, V. Ji, Effects of Co contents on the microstructures and properties of electrodeposited NiCo–Al composite coatings, Appl. Surf. Sci. 324 (2015) 482–489.
[38] R. Kaibyshev, I. Mazurina, D. Gromov, Mechanisms of grain refinement in aluminum alloys in the process of severe plastic deformation, Met. Sci. Heat Treat. 48 (2006) 57–62.
[39] X. Liu, A.P. Warren, N.T. Nuhfer, A.D. Rollett, K.R. Coffey, K. Barmak, Comparison of crystal orientation mapping-based and image-based measurement of grain size and grain size distribution in a thin aluminum film, Acta Mater. 79 (2014) 138–145.
[40] R. Fleischer, D. Dimiduk, H. Lipsitt, Intermetallic compounds for strong high-temperature materials: status and potential, Annu. Rev. Mater. Sci. 19 (1989) 231–263.
[41] L. Hu, J. Li, Y. Tao, Y. Lv, Corrosion behaviors of TiNi/Ti 2 Ni matrix coatings in the environment rich in Cl ions, Surf. Coating. Technol. 311 (2017) 295–306.
[42] N.D. Tomashov, Passivity and Protection of Metals Ag Corrosion, Springer Science & Business Media, 2012.
[43] B. Bakhit, A. Akbari, F. Nasirpouri, M.G. Hosseini, Corrosion resistance of Ni–Co alloy and Ni–Co/SiC nanocomposite coatings electrodeposited by sediment codeposition technique, Appl. Surf. Sci. 307 (2014) 351–359.
[44] K. Przybylski, W. Smeltzer, High temperature oxidation mechanism of CoO to Co_3O_4, J. Electrochem. Soc. 128 (1981) 897–902.
[45] E. Abdel-Aal, M.M. Rashad, Kinetic study on the leaching of spent nickel oxide catalyst with sulfuric acid, Hydrometallurgy 74 (2004) 189–194.
[46] S. Dey, A. Hazotte, E. Bouzy, Crystallography and phase transformation mechanisms in TiAl-based alloys–A synthesis, Intermetallics 17 (2009) 1052–1064.
[47] V. Aigbodion, A. Popoola, O. Fatoba, Evaluation of hardness values and corrosion behavior of laser alloyed 20Al-20Sn-60Ti on UNS G10150 mild steel, Int. J. Adv. Manuf. Technol. 86 (2016) 291–301.